Advective vertex-centered Reconstruction Scheme on unstructured Meshes

Hilde Ouvrard, Tatiana Kozubskaya, Ilia Abalakin, Bruno Koobus, Alain Dervieux

INRIA

INSTITUT NATIONAL DE RECHERCHE EN INFORMATIQUE ET EN AUTOMATIQUE

Advective vertex-centered Reconstruction Scheme on unstructured Meshes

H. Ouvrard, T. Kozubskaya, I. Abalakin, B. Koobus, A. Dervieux

N° 7033

Avril 2009

Thème NUM

apport de recherche

ISSN 0249-6399 ISRN INRIA/RR--7033--FR+ENG

Advective vertex-centered Reconstruction Scheme on unstructured Meshes

H. Ouvrard*, T. Kozubskaya†, I. Abalakin‡, B. Koobus§, A. Dervieux¶

Thème NUM — Systèmes numériques
Projet Pumas

Rapport de recherche n° 7033 — Avril 2009 — ?? pages

Abstract: We propose and experiment a reconstruction finite-volume scheme for vertex-centered unstructured meshes. The reconstruction is quadratic and 2-exact with respect to mean cell values. The quadrature formulas for fluxes are also exact for quadratic polynomial. The resulting scheme is third-order accurate. We evaluate its accuracy on advection test cases. We apply this method to the linearised Euler model and compare it to a superconvergent mixed-element-volume scheme.

Key-words: Computational Fluid Dynamics, finite volume, reconstruction, upwind, unstructured meshes, acoustics

* University of Montpellier II, France
† IMM, Miuskaya sq., 4a, Moscow 125047, Russia
‡ IMM, Miuskaya sq., 4a, Moscow 125047, Russia
§ University of Montpellier II, France
¶ INRIA, 2004 Route des Lucioles, BP. 93, 06902 Sophia-Antipolis, France

Unité de recherche INRIA Sophia Antipolis
2004, route des Lucioles, BP 93, 06902 Sophia Antipolis Cedex (France)
Téléphone : +33 4 92 38 77 77 — Télécopie : +33 4 92 38 77 65

Schéma advectif de reconstruction centrée-sommet sur des maillages non-structurés

Résumé : On propose et on expérimente un schéma advectif aux volumes finis avec reconstruction centrée s'appliquant à des maillages non-structurés. La reconstruction est quadratique et 2-exact par rapport aux valeurs moyennes sur les cellules. Les formules de quadrature pour les flux advectifs sont aussi exactes en quadratique. On évalue la précision sur des cas tests d'advection. On applique cette méthode d'approximation aux équations d'Euler lin]'earisées et on compare le schéma avec un schéma mixte-élément-volume superconvergent.

Mots-clés : Mécanique des Fluides Numérique,volumes finis, reconstruction, decentrage, maillages non-structurés, acoustique

1 Introduction

Deriving an approximation of Euler flows and, more generally of non-linear hyperbolic models is a delicate problem which has given business to many researchers. The main difficulties are shortly listed now:

(i)- High-order methods, with space and time order more than 3, are probably required.

(ii)- But many high-order methods are not sufficiently spatially stable for computing highly non-homogeneous or even singular solution fields, or similarly for applying irregular meshes.

(iii)- Many problems of interest involve also complex geometries, and many high-order methods cannot address this requirement.

(iv)- For 3D applications, high-order methods are interesting to apply on medium-size meshes only if the CPU consumption by degree of freedom is sufficiently small.

Due to the difficulty in stability, many investigations rely on discontinuous solution representation combined with Riemann solvers. We distinguish two families of high-order methods, both applying on unstructured meshes in order to address difficulty (iv).

- In (Weighted or not) Essentially Non Oscillating (ENO/WENO) methods, the unknown on cell is a spatial mean, but a high-order reconstruction in the cell is built with neighboring cell means.

- In Discontinuous Galerkin (DG) methods, the approximation relies on a canonic interpolation defined in each finite element.

Finite volume methods using reconstruction, like ENO, are more easy to introduce in existing software. The purpose of this paper is to develop a third-order accurate finite-volume scheme using unstructured grids. We shall follow some features of the ENO method. However, in order to have CPU efficiency, we shall introduce several simplifications.

The ENO (Essentially Non-Oscillatory) schemes, developed by Harten, Osher Engquist and Chakravarthy for two-dimensional unstructured grids are based on the construction of a polynomial approximation of the solution using several stencils and choosing the stencil which generate the smoothest polynomial. The smoothless of a polynom characterizes its oscillations. The WENO (Weighted Essentially Non-Oscillatory) schemes is obtained constructing a polynomial approximation in each stencils and using a weighted sum of all polynomials to construct a new polynom. It was design by Liu, Osher and Chan for one-dimensional problems is well adapted to capture shocks. Later improvement of Jiang and Shu in [?] leads to a WENO scheme twice as fast as classical ENO scheme by modifying the measure of smoothness .

However, because of the measure of smoothness on every stencil, the computational cost of WENO methods are still too high to be routinely applied to three-dimensional problems. Barth and Frederickson presented first in [?] the polynomial reconstruction using a fixed stencil, from many extension of basic ideas used on structured grids. Their high order accurate schemes have been designed to solve the Euler equations requiring a k-exact reconstruction. Barth in [?] improved this methods by decreasing the number of cells in the used stencil but it remains some conditioning problems for highly stretched grids. Delanaye and Essers in [?] presented a quadratic reconstruction with a high-order accurate flux evaluation with Gauss quadrature. This scheme has the characteristic to be high order accurate on very distorded grids so that adaptatived grids could be used.

The presented scheme is an adaptation of simplified ENO schemes of Carpentier. In [?], optimal choice for fixed order of accuracy are obtained for structured two-dimensional quadrangle grids.

Another important feature of our work is its vertex-centered formulation. Indeed, the degrees of freedom are attached to vertices and represent the mean of the unknown over the dual cell around

this vertex. This has some pros and cons which we shall discuss in the sequel. An easy-to-see advantage is that the number of degres of freedom (and therefore the number of reconstructions) is as small as possible for a given triangulation or, in 3D, tetrahedrization.

We introduce first the method by recalling the finite-volume method construction and the approximation process which consists of three steps, the reconstruction, the flux integration, and the time evolution. We then proceed to the numerical study of the scheme with two test cases of steady and unsteady convection and compare it to some scheme derived from another principle.

2 Simplified ENO reconstruction

We consider the hyperbolic equation:

$$\frac{\partial u}{\partial t}(x,y,t) + \nabla.\vec{f}(u(x,y,t)) = 0 \tag{1}$$

with boundary and initial conditions given by:

$$\begin{cases} u(x,y,t) & = \phi(x,y,t) \quad \text{for } (x,y) \in \partial\Omega \\ u(x,y,0) & = u_0(x,y) \end{cases}$$

where $(x,y) \in \Omega$ with Ω open set of $\mathbb{R}^2$, $t \geq 0$.
$u : \Omega \times \mathbb{R}_+^* \to \mathbb{R}$ and
$\vec{f}(u(x,t)) = (f_1(u(x,y,t), f_2(u(x,y,t))^t$ where $f_i \in \mathcal{C}^1(\mathbb{R},\mathbb{R})$
The spatial domain Ω is sub-divided into vertex centered control volumes or cells C_i constructed by connecting the midpoint of the edges and the center of gravity of the triangles containing the vertex i (see figure ??).

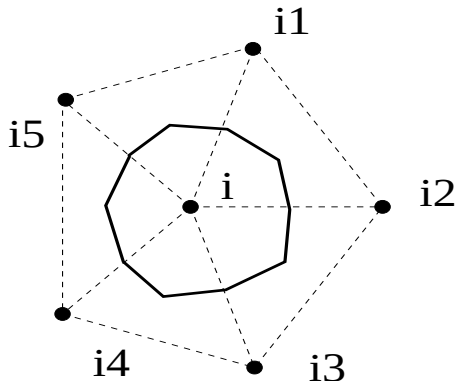

Figure 1: Construction of vertex-centered cell C_i

Finite-Volume Method

Integrating on every control volume C_i and using the Green's formula, one obtain:

$$\frac{d}{dt}\int_{C_i} u(x,y,t)dxdy + \int_{\partial C_i} \vec{f}(u(x,y,t)).\vec{n}ds = 0$$

where n is the local exterior normal of the cell C_i. The boundary of the cell C_i is polygonal and can be decomposed in the following way:

$$\frac{d}{dt}\int_{C_i} u(x,y,t)dxdy + \sum_{k\in V(i)} \int_{\partial C_i \cap \partial C_k} \vec{f}(u(x,y,t)).\vec{n}ds = 0$$

with $V(i)$ the set of neighbors of the vertex i.

Polynomial Reconstruction

On each control volume C_i and each timestep, we seek to approximate the solution $u(x,y,t^n) = u(x,y)^n$ by reconstructing a quadratic polynomial P_i^n.
It is required that the average of the polynomial P_i^n and of the solution on the cell C_i are equal. This condition can be written:

$$\overline{P_{i,i}^n} = \overline{u_i^n} \tag{2}$$

with

$$\overline{P_{i,i}^n} = \frac{1}{area(C_i)}\int_{C_i} P_i^n(x,y)dxdy$$

and

$$\overline{u_i^n} = \frac{1}{area(C_i)}\int_{C_i} u^n(x,y)dxdy$$

The polynomial $P_{i,i}^n$ is defined by:

$$P_i^n = \overline{u_i^n} + \sum_{\alpha\in I} c_{i,\alpha}^n \left[(X-X_{0,i})^\alpha - \overline{(X-X_{0,i})^\alpha}\right] \tag{3}$$

where

$$\overline{(X-X_{0,i})^\alpha} = \frac{1}{area(C_i)}\int_{C_i} (X-X_{0,i})^\alpha dxdy$$

$I = \{\alpha = (\alpha_1,\alpha_2) \in \mathbb{N}\times\mathbb{N}, |\alpha| = \alpha_1+\alpha_2 \in [1,2]\}$ is the set of multi-indices,
$(X-X_{0,i})^\alpha = (x-x_{0,i})^{\alpha_1}(y-y_{0,i})^{\alpha_2}$ where $(x_{0,i},y_{0,i})$ represents the center of gravity of the cells C_i.
In this way, the condition (**??**) is guaranteed.

To construct the polynomial P_i^n we need to define the stencil S_i formed from the cells around the vertex i in order to take enough values of the solution around i. The construction of the stencil S_i depends on the number of neighbors and on the logic boundary conditions of i. S_i always contains the cells C_k where k is a neighbor of i. To compute the 5 coefficients of the polynomial, we need at least 5 nodes. Consider an internal vertex i. If i has 5 and more neighbors, the stencil S_i is formed from the cells centered on the neighbors of i. Otherwise the stencil S_i contains the cells C_k and the cells C_l too, where l is a neighbor of k and k a neighbor of i (see Figure **??**).

The 5 coefficients unknown $c_{i,\alpha}^n$ of the reconstructed polynomial have to be found so that the L_2 distance between the average of the polynomial on a cell C_k and the average of the solution $\overline{u_k^n}$

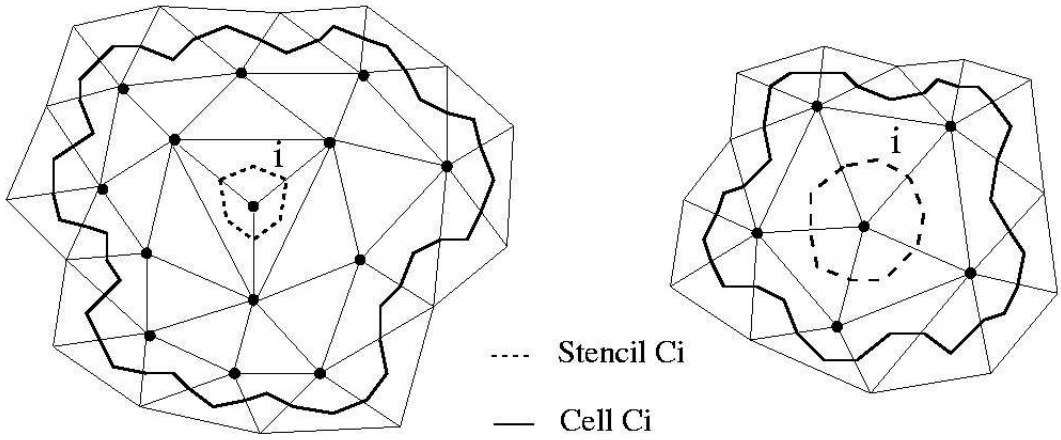

Figure 2: Construction of an internal Stencil S_i

is minimum for each vertex k included in the stencil S_i. It amounts to minimising the following fonction,

$$H_i = \sum_{k \in N(i)} (\overline{P^n_{k,i}} - \overline{u^n_i})^2 \tag{4}$$

where $\overline{P^n_{k,i}}$ represents the average of the polynomial P^n_i on the cell k.

$$\overline{P^n_{k,i}} = \frac{1}{area(C_k)} \int_{C_k} P^n_i(x,y)dxdy$$

By construction of C_k, it can be written:

$$H_i = \sum_{k \in N(i)} (\frac{1}{area(C_k)} \sum_{T \in C_k} \int_T P^n_i(x,y)dxdy - \overline{u^n_i})^2$$

This leads to the least square problem:

$$M_i c^n_i = b^n_i$$

M_i is a symmetric 5×5 matrix with,

$$(M_i)_{1 \le p,q \le 5} = \sum_{C_k \in N_i} D_{i,k,p} D_{i,k,q}$$

$$D_{i,k,\alpha} = \frac{1}{area(C_k)} \sum_{T \in C_k} \int_T (X - X_{0,i})^\alpha dxdy - \frac{1}{area(C_i)} \sum_{T \in C_i} \int_T (X - X_{0,i})^\alpha dxdy$$

c_i^n is the column vector of the unknown coefficients:

$$c_i^n = \begin{pmatrix} c^n_{i,(1,0)} \\ c^n_{i,(0,1)} \\ c^n_{i,(1,1)} \\ c^n_{i,(2,0)} \\ c^n_{i,(0,2))} \end{pmatrix}$$

The right hand side b_i^n is a column vector depending on the average of the solution $\overline{u_k^n}$ on the neighborhood of the vertex i with:

$$b^n_{i,p} = \sum_{k \in N(i)} (\overline{u_k^n} - \overline{u_i^n}) D_{i,k,p} \quad \text{for } p = 1..5 \tag{5}$$

The integrals of the monomials $\int_T (X - X_{0,i})^\alpha$ contained in the matrix are computed by Gauss point quadrature.

On the reference triangle formed from the nodes $(0,0)$, $(0,1)$ and $(1,0)$, the weighted sum on the points $(0, \frac{1}{2})$, $(\frac{1}{2}, 0)$ and $(\frac{1}{2}, \frac{1}{2})$ with weights equal to $\frac{1}{3}$ yields an exact approximation of the monomials.

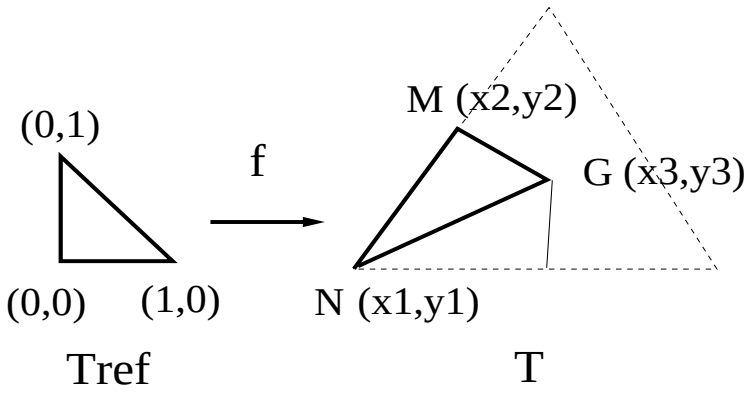

Figure 3: Affine transformation f

The affine transformation f (see figure **??**) which transform the triangle $Tref$ into a triangle T formed from a node $N(x_1, y_1)$, a midpoint $M(x_2, y_2)$ of a segment and a center of gravity $G(x_3, y_3)$ of a triangle of the grid is defined by:

$$f : \begin{pmatrix} x' \\ y' \end{pmatrix} \to \begin{pmatrix} f_1(x', y') \\ f_2(x', y') \end{pmatrix} = \begin{pmatrix} x_2 - x_1 & x_3 - x_1 \\ y_2 - y_1 & y_3 - y_1 \end{pmatrix} \begin{pmatrix} x' \\ y' \end{pmatrix} + \begin{pmatrix} x_1 - x_{0,i} \\ y_1 - y_{0,i} \end{pmatrix}$$

Applying the substitution rule to come down to the integral on the triangle $Tref$ yields:

$$\int_T (X - X_{0,i})^\alpha = 2area(T) \int_{Tref} f_1(x', y')^{\alpha_1} f_2(x', y')^{\alpha_2} dx' dy'$$

since the absolute value of the Jacobian determinant of the transformation f is $2vol(T)$. Then applying a 3-points Gauss quadrature rule gives:

$$\int_T (X - X_{0,i})^\alpha = area(T) \sum_{g=1}^{3} \omega_g f_1(x'(g), y'(g))^{\alpha_1} f_2(x'(g), y'(g))^{\alpha_2}$$

where $(x'(g), y'(g))$ are the coordinates of the gauss points in the triangle T for $g \in \{1, 2, 3\}$.

As the used unstructured grid is fixed, the value of the integrals doesn't depend on timestep and thus the matrix M_i have to be computed once for each node i. In order to use the symmetry, its inverse M_i^{-1} is computed with the Bunch-Kaufman algorithm at the first time step and is stored for the next steps.

Flux Evaluation

Our next objective is to evaluate the flux at the time t on the interfaces between the cell C_i and its neighbors C_k for all k in $V(i)$ using a Gauss quadrature.

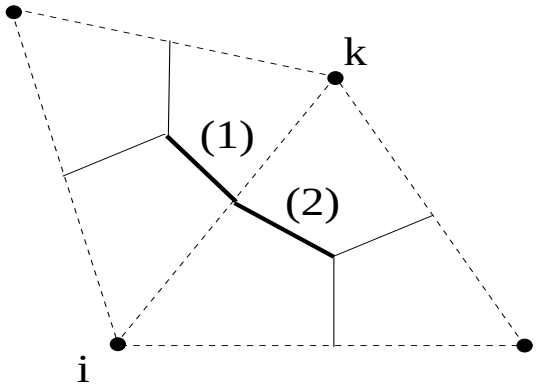

Figure 4: Interfaces between C_i and C_k, $(1) : \partial C_{ik}^{(1)}$ and $(2) : \partial C_{ik}^{(2)}$

Reminding that the flux on the boundary of the cell C_i can be written:

$$\int_{\partial C_i} \vec{f}(u(x,y,t)).\vec{n}ds = \sum_{k \in V(i)} \int_{\partial C_i \cap \partial C_k} \vec{f}(u(x,y,t)).\vec{n}ds$$

the interfaces $\partial C_i \cap \partial C_k$ can be decomposed in two segments $\partial C_{ik}^{(1)}$ and $\partial C_{ik}^{(2)}$, see figure **??**.

$$\int_{\partial C_i \cap \partial C_k} \vec{f}(u(x,y,t)).\vec{n}ds = \sum_{l=1,2} \int_{\partial C_{ik}^{(l)}} \vec{f}(u(x,y,t)).\vec{n}ds$$

The solution $u(x, y, t)$ on the cell C_i is approximated by the polynomial P_i constructed in the previous section:

$$\int_{\partial C_{ik}^{(l)}} \vec{f}(u(x,y,t)).\vec{n}ds \approx \int_{\partial C_{ik}^{(l)}} \vec{f}(P_i(x,y,t)).\vec{n}ds$$

Then, the integral on each segments $C_{ik}^{(l)}$ is evaluated by a Gauss quadrature with 2 points $(x_{g_1,ik}^{(l)}, y_{g_1,ik}^{(l)})$ and $(x_{g_2,ik}^{(l)}, y_{g_2,ik}^{(l)})$.

On the reference segment $[-1,1]$, the gauss points $\pm\frac{1}{\sqrt{3}}$ give an exacte approximation of a quadratic polynomial with weights $\omega_{1,2} = 1/2$. After an affine transformation on the reference segment and a 2-points Gauss quadrature rule, one obtain:

$$\int_{\partial C_{ik}^{(l)}} \vec{f}(P_i(x,y,t)).\vec{n}ds = \sum_{m=1,2} \omega_m \vec{f}(P_i(x_{g_m,ik}^{(l)}, y_{g_m,ik}^{(l)}, t))\vec{\nu_{ik}}^{(l)}$$

with $\nu_{ik}^{(l)} = \int_{\partial C_{ik}^{(l)}} \vec{n}(x,y)ds$

Because two distinct polynomials P_i and P_k have been constructed, the solution on the Gauss points of the boundary is not unique. So, the flux on the interface $\partial C_{ik}^{(l)}$ is approximate by a numerical flux fonction Φ :

$$\vec{f}(P_i(x_{g_m,ik}^{(l)}, y_{g_m,ik}^{(l)}, t)).\vec{n} \approx \Phi(P_i(x_{g_m,ik}^{(l)}, y_{g_m,ik}^{(l)}, t), P_k(x_{g_m,ik}^{(l)}, y_{g_m,ik}^{(l)}, t), \vec{\nu_{ik}})$$

where $\vec{\nu_{ik}} = \int_{\partial C_i \cap \partial C_k} \vec{n}(x)dx$ is a constant vector since the grid is fixed.
We have to choose the numerical flux Φ such as the resulting scheme is stable, for exemple the Roe scheme:

$$\Phi(u_1, u_2, \vec{\nu}) = \frac{\vec{f}(u_1) + \vec{f}(u_2)}{2}.\vec{\nu} - \frac{\gamma}{2}\left|\frac{\partial \vec{f}}{\partial u}\left(\frac{u_1+u_2}{2}\right).\vec{\nu}\right|(u_2 - u_1)$$

$\gamma \in [0,1]$ is a parameter we are able to control the numerical viscosity with.

2.1 Evolution

The semi-discretization in space of the equation (**??**) leads to the following ODE system:

$$\frac{du_i(t)}{dt} + \Psi_i(u(t)) = 0 \tag{6}$$

where the function $\Psi_i(u(t))$ approximates $\nabla.\vec{f}(u(x,y,t))$ at point (x_i, y_i) and $\{u(t)\}$ is the set of the averages $\overline{u_k^n}$ where k is in the neighborhood of i, refering to expression (**??**) and to the right hand side (**??**) of the least square matrix.
We choose the N-step explicite Runge Kutta method for the discretisation in time:

$$\begin{cases} u_i^{(0)} & = u_i^n \\ u_i^{(\alpha)} & = u_i^{(0)} - \dfrac{\Delta t}{N+1-\alpha}\Psi_i(u_i^{(\alpha-1)}) \quad \text{for } \alpha = 1..N \\ u_i^{n+1} & = u_i^N \end{cases}$$

3 Analysis of the scheme

3.1 Truncation analysis

One considers the two-dimensional linear advection equation:

$$\frac{\partial u}{\partial t}(x,y,t) + a\frac{\partial u}{\partial x}(x,y,t) + b\frac{\partial u}{\partial y}(x,y,t) = 0 \tag{7}$$

We apply the scheme to a Cartesian mesh of Friedrichs-Keller type, that is made of squares split in triangles with diagonals of only one direction, see Fig. **??**. A space-wise modified equation analysis

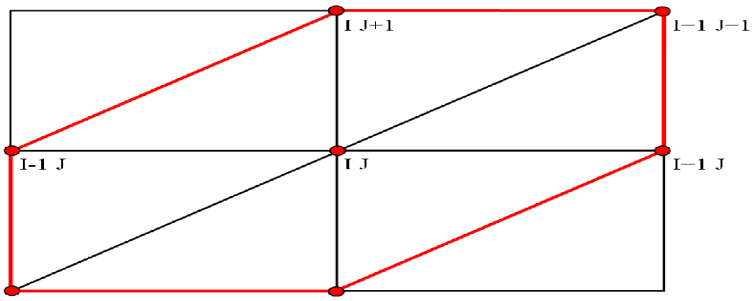

Figure 5: Friedrichs-Keller cartesian triangulation

gives:

$$\begin{aligned} a\frac{\partial u}{\partial x} + b\frac{\partial u}{\partial y} \quad = \quad & \\ & -|a|\frac{1}{12}\frac{\partial^4 u}{\partial x^4}\Delta x^3 - |a|\frac{1}{12}\frac{\partial^4 u}{\partial x^3 \partial y}\Delta x^2 \Delta y - |a|\frac{1}{12}\frac{\partial^4 u}{\partial x^2 \partial y^2}\Delta x \Delta y^2 \\ & -|b|\frac{1}{12}\frac{\partial^4 u}{\partial y^4}\Delta y^3 - |b|\frac{1}{12}\frac{\partial^4 u}{\partial x \partial y^2}\Delta x \Delta y^2 - |b|\frac{1}{12}\frac{\partial^4 u}{\partial y^2 \partial x^2}\Delta x^2 \Delta y \\ & +O(\Delta x^4, \Delta y^4) \end{aligned}$$

Truncation error is of order three independantly of the ratio between Δx and Δy. This can be put in contrast with the analogous analysis of the Mixed-Element-Volume scheme of [**?**] for which unconsistent terms appear for high aspect ratio.

3.2 Stability study in 1D case

One considers the unidimensional advection equation:

$$\frac{\partial u}{\partial t}(x,t) + \frac{\partial}{\partial x}(f(u(x,t))) = 0 \tag{8}$$

This study is restricted to the case

$$f(u(x,t) = vu(x,t)$$

with v the advection velocity, using a regular mesh: $x_{j+1} - x_j = \Delta x, \forall j$. The convective term is discretized with a finite-volume method. The control cell C_j associated to the node j is defined by $C_j = [x_{j-\frac{1}{2}}; x_{j+\frac{1}{2}}]$ with $x_{j\pm\frac{1}{2}} = \frac{x_j + x_{j\pm1}}{2}$.

Integrating equation (??) gives for each nodes i:

$$\frac{d}{dt}\int_{C_j} u(x,t) + \int_{\partial C_j} v.u(x,t)\vec{n}d\sigma = 0$$

We seek to approximate the convectif term by an operator L depending of the mean values at nodes j and its neighbors.

$$\int_{\partial C_j} v.u(x,t)\vec{n}d\sigma = \frac{1}{\Delta x}(\Phi_{x_{j+\frac{1}{2}}} - \Phi_{x_{j-\frac{1}{2}}}) = \frac{1}{\Delta x}\left[\Phi(P_j(x_{\frac{j+1}{2}}), P_{j+1}(x_{\frac{j+1}{2}})) - \Phi(P_{j-1}(x_{\frac{j-1}{2}}), P_j(x_{\frac{j-1}{2}}))\right]$$

$\Phi_{x_{j+\frac{1}{2}}}$ and $\Phi_{x_{j+\frac{1}{2}}}$ approximating the flux at the interfaces between the cell C_j and its neighoring cells C_{j-1} and C_{j+1}, Φ is the Roe flux as described previously and P_k the reconstructed polynomial in the cell C_k.

As explain previously, the quadratic polynomial must verify the criteria (??) and minimize the fonctional (??), which leads to a matricial equation where the unknowns $c_j = (c_{j1}, c_{j2})$ are the coefficient of the polynomial P_j to be found. Solving this equation yields for each nodes j:

$$P_j(x) = \overline{u}_j + \frac{1}{2\Delta x}(\overline{u}_{j-1} - \overline{u}_{j+1})(x - x_j) + \frac{1}{2\Delta x^2}(-\overline{u}_{j-1} + 2\overline{u}_j - \overline{u}_{j+1}\left[(x - x_j)^2 - \frac{1}{12}\Delta x^2\right]$$

Thus the operator L can be written:

$$L = \frac{v}{2\Delta x}\left[\frac{1}{6}(\overline{u}_{j+2} - \overline{u}_{j-2}) + \frac{2}{3}(\overline{u}_{j+1} - \overline{u}_{j-1})\right] - \frac{\gamma v}{2\Delta x}\left[\frac{1}{6}(\overline{u}_{j+2} + \overline{u}_{j-2}) + \frac{4}{3}(\overline{u}_{j+1} + \overline{u}_{j-1}) - 3\overline{u}_j\right]$$

3.3 Explicit time advancing

The stability of the quasi-ENO scheme is studied using the Von Neumann stability analysis. Including a Fourier mode $\hat{u}_j^n = \overline{u}_k^n e^{ij\theta_k}$ in equation (??) gives:

$$L = \frac{v}{6\Delta x}\Big[-\gamma\left[cos(2\theta) + 8cos(\theta) - 9\right] + i\left[sin(2\theta) + 4sin(\theta)\right]\Big]\hat{u}_j$$

Let us define the gain fonction $G_\theta = g(z_\theta)$ with $z_\theta = \lambda_\theta \Delta t$.
g is the characteristic polynomial of the Runge Kutta 4 method:

$$g(z) = 1 + z + \frac{z^2}{2} + \frac{z^3}{6} + \frac{z^4}{24}$$

λ_θ is a linear operator verifying $L = -\lambda_\theta \hat{u}_j^n$ and Δt the time step. We introduce the courant number ν. The figure ?? shows the behaviour of the function $g(\nu) = \max_{\theta\in[0,\pi]} \|G_\theta\|$ for different values of γ. In both case, we determinate the maximum value ν_{max} which verify the stability criterion, that is: $g(\nu) < 1$.
ν_{max} is equal to 1 and 3.1 for γ respectively equal to 1 and 0.3.
For both value of γ and corresponding ν_{max} value, figure ?? presents the behaviour of the amplification function $|G(\theta)|$ for different frequences $\theta \in [0, 2\pi]$.

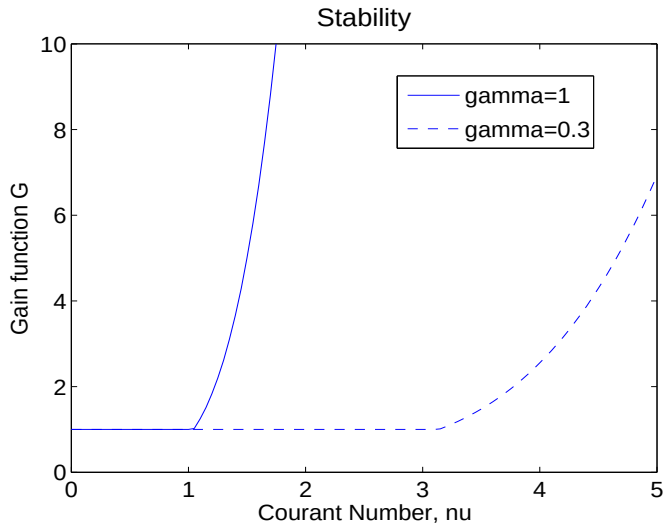

Figure 6: Stability of the scheme

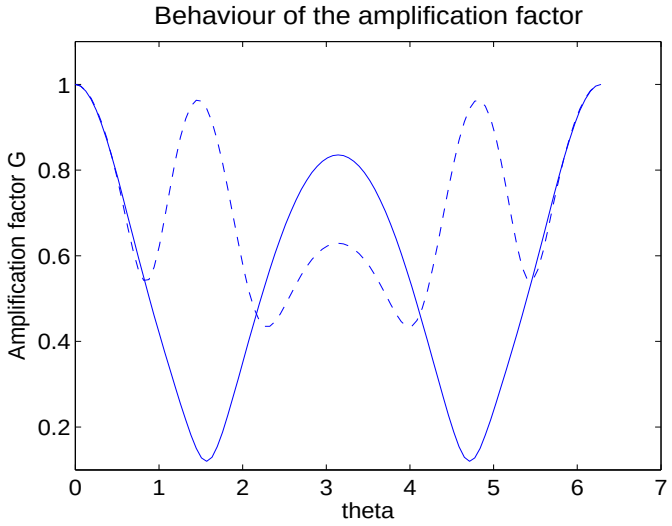

Figure 7:

3.4 First order implicit time advancing

Considering the first order implicit Steger Warming time stepping, discretization of equation ?? can be written:

$$T^n \delta \overline{U}^{n+1} = \Delta t^n L(\overline{U}^n)$$

where $\delta\overline{U}^{n+1} = \overline{U}^{n+1} - \overline{U}^{n}$ and T^n is the tridiagonale matrix of the implicit Steger Warming scheme.
With a classical Fourier analysis, one obtain an amplification factor equal to:

$$G(\Delta t) = \frac{t_\theta + z_\theta}{t_\theta}$$

with z_θ discribed as previously and $t_\theta = 1 + \nu(1 - cos(\theta)) + i\nu sin(\theta)$.
We observe in figure **??** the behaviour of this amplification factor when the time step Δt goes to ∞. In particular, we are interested by the value which maximize this limit $\max_\theta \left| \lim_{\Delta t \to \infty} G(\Delta t) \right|$. This maximum is equal to 0.53 and 0.34 for γ respectively equal to 1 and 0.3.

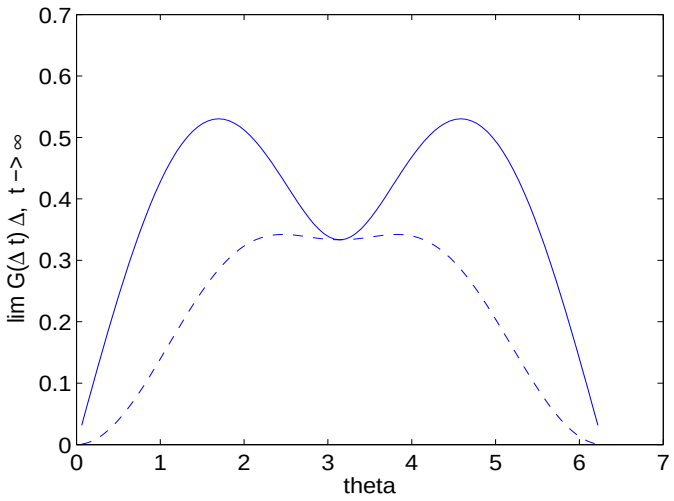

Figure 8: Limit of amplification factor, implicit case

4 Numerical results

In this section we present some numerical results in order to confirm the accuracy order of the scheme described in the previous section.

4.1 Unsteady convection

The first test problem consists of a two dimensional advection equation in the square $\Omega = [0, 1] \times [0, 1]$:

$$\frac{\partial u}{\partial t}(x, y, t) + \nabla.(\vec{V}u(x, y, t)) = 0$$

with a steady velocity field $\vec{V} = (1, 0)^t$.
The boundary conditions and initial conditions are given by:

$$\begin{cases} u(x, y, t) & = 1 \quad \text{for } (x, y) \in \partial\Omega \\ u(x, y, 0) & = 1 + e^{-75((x-\frac{1}{2})^2+(y-\frac{1}{2})^2)} \end{cases}$$

according to the notation in the previous section, $u_0(x, y)$ is a Gaussian function centered on the point of coordinates $(0.5, 0.5)$.

The Gaussian translation test case is computed on several unstructured and structured grids (see Table ?? and Table ??). $G2_{uns}$, $G3_{uns}$ and $G4_{uns}$ and respectively $G2_s$, $G3_s$ and $G4_s$ are constructed using grid divisions of $G1_{uns}$ and respectively $G1_s$, see Figure ??.

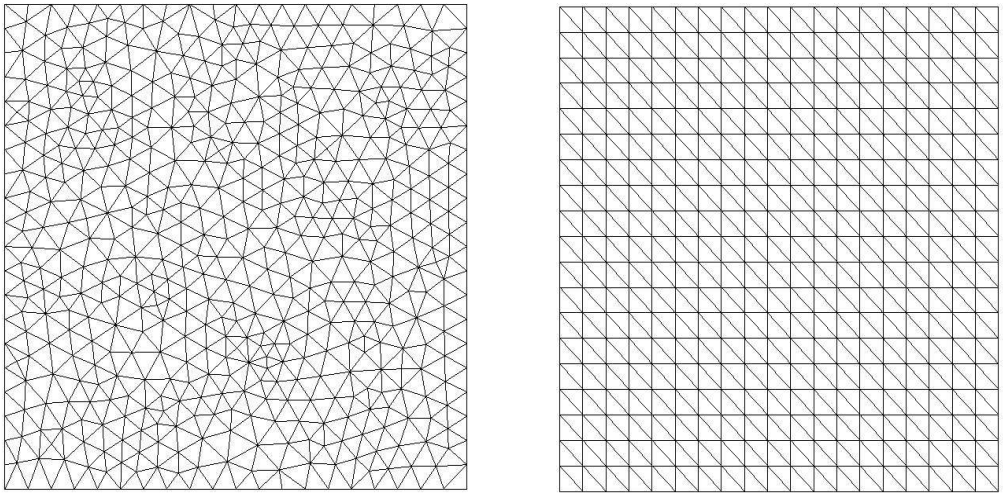

(a) coarsest unstructured grid

(b) coarsest structured grid

Figure 9: Meshes $G1_{uns}$ and $G1_s$

The analytical solution of this problem is: $u(x, y, t) = 1 + e^{-75((x-t-\frac{1}{2})^2+(y-\frac{1}{2})^2)}$. Using a grid fine enough, we notice that the shape of the translated Gaussian is rather well preserved (see Figure ??).

	$G1_{uns}$	$G2_{uns}$	$G3_{uns}$	$G4_{uns}$
nodes	535	2057	8065	31937

Table 1: Nodes number of the unstructured grids

	$G1_s$	$G2_s$	$G3_s$	$G4_s$
nodes	400	1521	5929	23409

Table 2: Nodes number of the structured grids

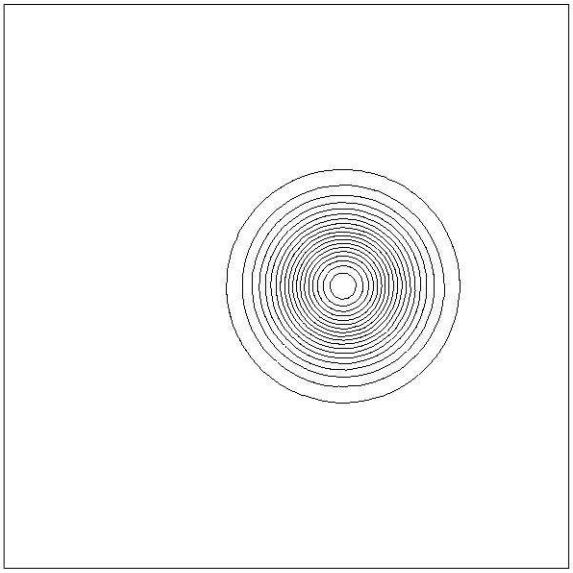

Figure 10: Translated Gaussian using $G3_{uns}$

To verify that the expected third-order accuracy is obtained, we need to quantify the accuracy of the computation. We evaluate the $L1$-error between the averaged exact and averaged computed solution using the differents grids, with $CFL = 0.1$ (non-optimized), a numerical viscosity $\gamma = 1$ and 4-step Runge Kutta explicite for the discretization in time. The plots on Figure **??** shows clearly that the order of accuracy of both cases is quite close. The actual order of accuracy computed using the two finest grids is 2.90 for the unstructured case and 2.95 for the structured case.

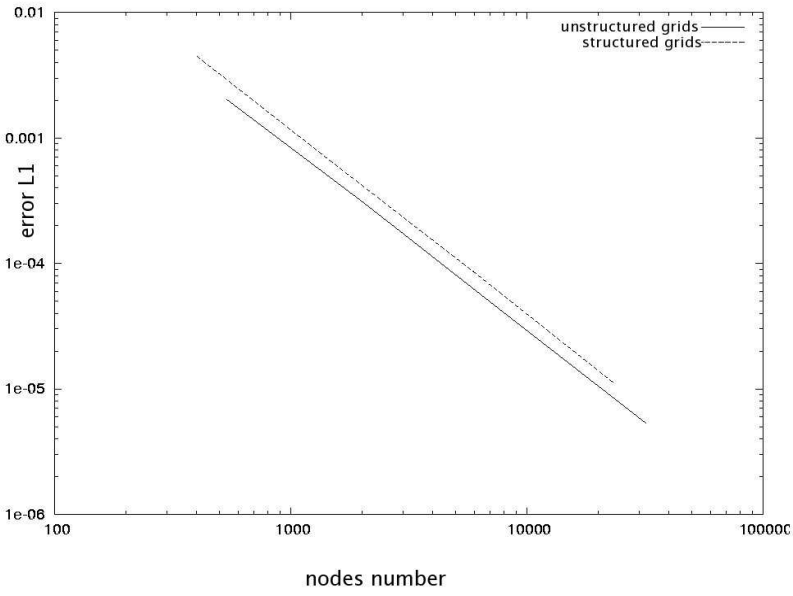

Figure 11: Convergence of the scheme

5 Application to acoustics

The quadratic reconstruction finite volume scheme, which we denote in short **QRFV**, is now compared to a few variants of the Mixed-Element-Volume (MEV) approximation. This approximation is described in [?] and is used for acoustics[?],[?], as well as for Large Eddy Simulation [?], [?]. This scheme is also vertex-centered and can be applied with two kinds of dual cells. Either the median cells already described in this paper are used. Or cells can be built, according to [?], by joining the center of circumcenter circle. The MEV schemes are also experimented under two versions. MEV3 is third-order accurate on regular meshes and involves a dissipative term designed on fourth-order spatial derivatives. MEV5 is fifth-order accurate on regular meshes and involves a dissipative term designed on sixth-order spatial derivatives.

The test case choosen addresses acoustic wave propagation. The challenge is to get a good accuracy for a rather large mesh size. We solve the linearized unsteady Euler equations in the 2D plane, with a stagnating reference flow of uniform density and pressure. Further details on this test case can be found in [?].

The initial conditions are as follows:

$$\rho(x,y,0) = Ae^{-\frac{\ln(2)}{b^2}(x^2+y^2)}$$

$$p(x,y,0) = Ae^{-\frac{\ln(2)}{b^2}(x^2+y^2)}$$

$$u(x,y,0) = v(x,y,0) = 0.$$

The parameter b defines the thickness of the Gaussian profile and is refered as the half-width. Starting from this perturbation, the linearised Euler equations are solved from time 0 to 40 in a square. At boundaries a non-reflecting boundary condition is applied. The numerical convergence order is evaluated from two different domain discretizations, with 100×100 cells (grid G1) and 200×200 cells (grid G2) and by comparison to the exact solution.

An example of density field obtained for this test case is depicted in Fig. ??.

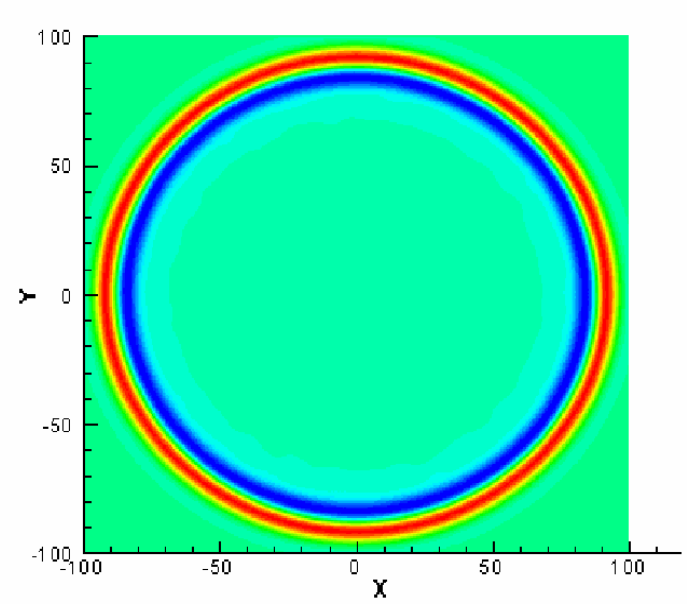

Figure 12: Density field of test case solution at time $T = 40$.

5.1 Comparison on a Cartesian mesh

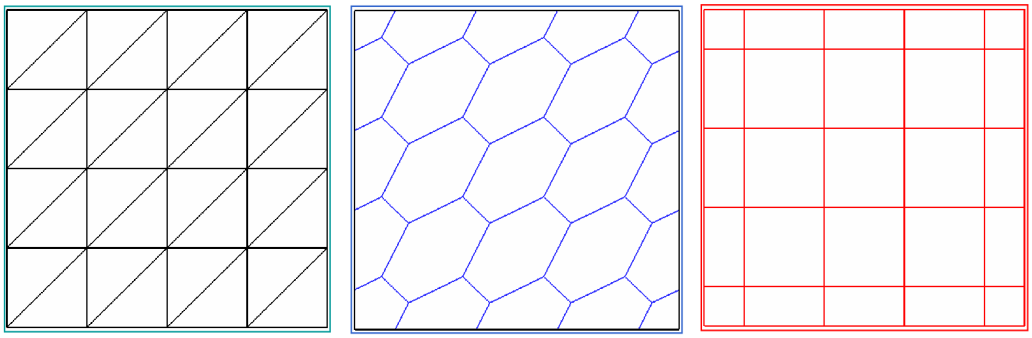

Figure 13: The Cartesian Friedrichs-Keller triangulation (left) with the median-based dual partition in cells (center) and the circumcenter dual partition (right).

	Mesh 1 ("Cartesian")				
Scheme	QRFV	MEV3	MEV3	MEV5	MEV5
Cells	median	median	circumcenter	median	circumcenter
	Impulse half-width $b = 3$				
G1: Error L_1	2.003D-3	2.028D-3	1.282D-3	1.228D-3	9.734D-4
G2: Error L_1	7.49405D-4	7.50928D-4	2.26015D-4	1.75957D-4	1.01179D-4
Order L_1	**1.42**	**1.43**	**1.65**	**2.80**	**3.27**
G1: Error L_2	5.10226D-3	5.12218D-3	2.78384D-3	3.11130D-3	2.44941D-3
G2: Error L_2	2.17870D-3	2.16434D-3	5.36623D-4	5.71060D-4	3.10311D-4
Order L_2	**1.23**	**1.24**	**1.48**	**2.45**	**2.98**
	Impulse half-width $b = 6$				
G1: Error L_1	1.30452D-3	1.28290D-3	1.75270D-3	2.72683D-4	1.51895D-4
G2: Error L_1	2.38422D-4	2.26015D-4	5.58635D-4	1.22426D-5	6.16242D-6
Order L_1	**2.45**	**2.50**	**2.65**	**4.48**	**4.62**
G1: Error L_2	2.85611D-3	2.78384D-3	4.49207D-3	6.65695D-4	3.40103D-4
G2: Error L_2	5.73216D-4	5.36623D-4	1.60635D-3	3.26011D-5	1.36763D-5
Order L_2	**2.32**	**2.38**	**2.58**	**4.35**	**4.64**

Table 3: Numerical convergence, Cartesian meshes

In Fig.**??**, the regularity of the mesh allows in principle for a nominal convergence of the different schemes, i.e. third order for QRFV, third order for MEV3, fifth order for MEV5. We have a confirmation that QRFV is close to third order, and of quality equivalent to MEV3.

5.2 Comparison on quasi-uniform acute mesh

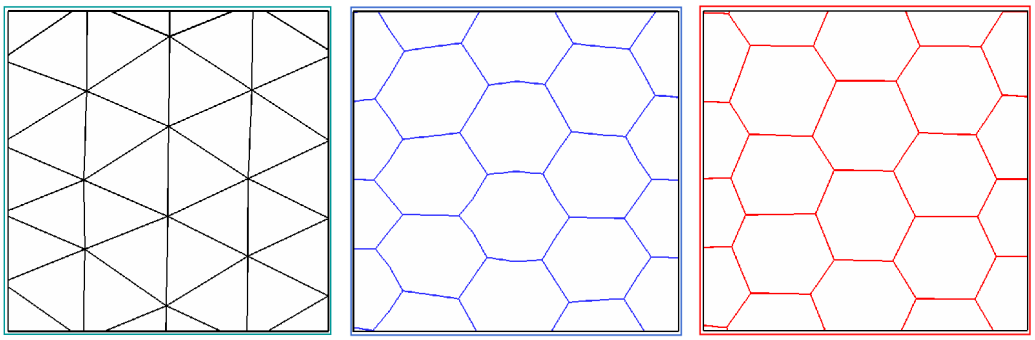

Figure 14: A quasi-uniform triangulation made of triangles close to unilateral ones (left), with the median-based dual partition in cells (center) and the circumcenter dual partition (right).

	Mesh 2 ("acute")				
Scheme	QRFV	MEV3	MEV3	MEV5	MEV5
Cells	median	median	circumcenter	median	circumcenter
	Impulse half-width $b = 3$				
G1: Error L_1	2.05374D-3	2.07351D-3	2.05986D-3	1.26700D-3	1.25677D-3
G2: Error L_1	6.94321D-4	7.08137D-4	7.05450D-4	1.50916D-4	1.50259D-4
Order L_1	**1.57**	**1.55**	**1.55**	**3.07**	**3.06**
G1: Error L_2	5.12439D-3	5.14155D-3	5.10924D-3	3.10037D-3	3.07297D-3
G2: Error L_2	1.92410D-3	1.94878D-3	1.94248D-3	4.24572D-4	4.25115D-4
Order L_2	**1.41**	**1.40**	**1.40**	**2.87**	**2.85**
	Impulse half-width $b = 6$				
G1: Error L_1	1.27860D-3	1.25865D-3	1.26898D-3	3.37566D-4	3.73845D-4
G2: Error L_1	1.99956D-4	1.93435D-4	1.95818D-4	4.28240D-5	5.07241D-5
Order L_1	**2.68**	**2.70**	**2.70**	**2.98**	**2.88**
G1: Error L_2	2.63185D-3	2.55384D-3	2.57485D-3	7.14735D-4	8.18106D-4
G2: Error L_2	4.34542D-4	4.14520D-4	4.20722D-4	9.66220D-5	1.22168D-4
Order L_2	**2.60**	**2.62**	**2.61**	**2.89**	**2.74**

Table 4: Numerical convergence, quasi-equilateral meshes.

Now the mesh is not strictly regular. Further, the mean triangle is about equilateral. In Fig.**??**, we observe that QRFV performs even better than with the cartesian one. The convergence order is close to the one of MEV3, yet less good than the one of MEV5.

5.3 Comparison on a quasi-uniform obtuse mesh

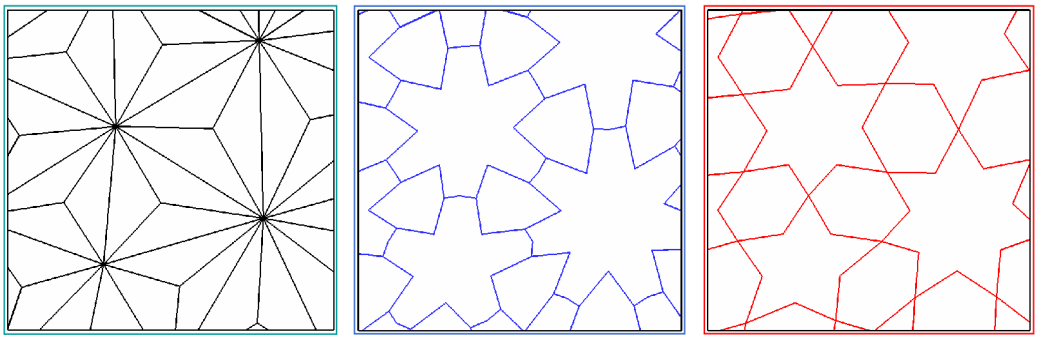

Figure 15: A quasi uniform triangulation with obtuse angles (left) with the median-based dual partition in cells (center) and the circumcenter dual partition (right)

	Mesh 3 ("Obtuse")				
Scheme	QRFV	MEV3	MEV3	MEV5	MEV5
Cells	median	median	circumcenter	median	circumcenter
	Impulse half-width $b = 3$				
G1: Error L_1	2.95893D-3	2.55823D-3	1.96222D-3	1.92949D-3	1.46617D-3
G2: Error L_1	1.17969D-3	1.09861D-3	7.73606D-4	5.99179D-4	3.72206D-4
Order L_1	**1.33**	**1.22**	**1.34**	**1.69**	**1.98**
G1: Error L_2	6.98447D-3	6.17985D-3	4.85346D-3	4.55210D-3	3.63613D-3
G2: Error L_2	3.13408D-3	2.88078D-3	2.10095D-3	1.62155D-3	1.05712D-3
Order L_2	**1.16**	**1.10**	**1.21**	**1.49**	**1.78**
	Impulse half-width $b = 6$				
G1: Error L_1	3.10978D-3	2.08162D-3	1.14894D-3	8.41003D-4	6.76269D-4
G2: Error L_1	4.90752D-4	3.84567D-4	2.25708D-4	2.04542D-4	1.10057D-4
Order L_1	**2.66**	**2.44**	**2.35**	**2.04**	**2.62**
G1: Error L_2	5.92167D-3	4.07593D-3	2.31742D-3	1.67667D-3	1.45982D-3
G2: Error L_2	1.09605D-3	8.10726D-4	4.86342D-4	4.37973D-4	2.44700D-4
Order L_2	**2.43**	**2.33**	**2.25**	**1.94**	**2.58**

Table 5: Numerical convergence, obtuses meshes

In Fig. **??**, we observe that MEV schemes are penalized by the irregular mesh. the new scheme produce still about the same convergence order, confirming its tolerance to mesh irregularity and to obtuse angles.

6 Conclusion

We have constructed and tested a vertex-centered finite-volume scheme with quadratic reconstruction. The scheme is theoretically 2-exact. Its truncation analysis shows a complete consistency, i.e. a much better behavior than usual vertex-centered finite volume schemes.

We have applied it to several two-dimensional advection test cases. The new scheme is about three times more expansive than the second-order vertex-centered finite volume scheme. The scheme shows third-order asymptotical accuracy.

This scheme has been also applied to a classical 2D test case in acoustics. Quasi-regular meshes are used. On these meshes, another family of schemes has been specially adapted. As can be expected, the new scheme is not better, but shows a reasonable accuracy.

On strongly non-uniform meshes, the vertex-centered finite volume schemes gives oscillatory solutions while the proposed scheme keeps some quality.

References

[1] T. Barth. Aspects of Unstructured Grids and Finite-Volume Solvers for the Euler and Navier-Stokes Equations, in *Special Course on Unstructured Grid Methods for Advection Dominated Flows, AGARD report 787*, p. 6-1 to 6-61, 1992.

[2] T.J. Barth. Recent developments in high order k-exact reconstruction on unstructured meshes. *AIAA JOURNAL*, january 1993.

[3] C.O.E Burg. Higher order variable extrapolation for unstructured finite volume rans flows solvers. *AIAA JOURNAL*.

[4] M. Van Altena and C. Ollivier-Gooch. A high-order-accurate unstructured mesh finite-volume scheme for the advection-diffusion equation. *Journal of Computational Physics*, (181):729–752, february 2002.

[5] R. Carpentier. Schema de haute precision en maillage quadrangulaire structure pour des ecoulements compressibles non visqueux. *Rapport INRIA*, (3909), April 2000.

[6] C. Debiez. *Approximation et linearisation d'ecoulements aerodynamiques instationnaires*. PhD thesis, Universite de Nice Sofia-Antipolis, decembre 1996.

[7] M. Delanaye and J.A. Essers. Quadratic-reconstruction finite volume scheme for compressible flows on unstructured adaptative grids. *AIAA JOURNAL*, 35:631–639, April 1997.

[8] C.W Shu and G.S Jiang. Efficient implementation of weighted eno schemes. *Journal of Computational Physics*, 126(202-228), january 1996.

[9] G. Strang. Accurate partiel difference methods. *Numerische Mathematik*, 6:37–46, 1964.

[10] C. Ollivier-Gooch. Quasi-eno schemes for unstructured meshes based on unlimited data-dependent least-squares reconstruction. *Journal of Computational Physics*, (133):6–17, september 1996.

[11] P.O. Frederickson T.J. Barth. High order solution of the euler equations on unstructured grids using quadratic reconstruction. *AIAA Paper* No. 90-0013, january 1990.

[12] C. Debiez, A. Dervieux. Mixed Element Volume MUSCL methods with weak viscosity for steady and unsteady flow calculation. *Computers and Fluids*, 1999,**29**, 89-118

[13] I. Abalakin, A. Dervieux and T. Kozubskaya, "A vertex centered high order MUSCL scheme applying to linearised Euler acoustics", *INRIA*, RR-4459 (2002)

[14] S. Camarri, M.-V. Salvetti, A. Dervieux and B. Koobus, "A low diffusion MUSCL scheme for LES on unstructured grids", *INRIA*, RR-4512, Juillet 2002

[15] N. Gourvitch, G. Roge, I. Abalakin, A. Dervieux and T. Kozubskaya, "A tetrahedral-based superconvergent scheme for aeroacoustics" *INRIA*, RR-5212, Projet Smash, May 2004

[16] Bruno Koobus, Stephen Wornom, Simone Camarri, Maria-Vittoria Salvetti, Alain Dervieux, "Nonlinear V6 schemes for compressible flow", *INRIA*, RR-6433(2008)

Unité de recherche INRIA Sophia Antipolis
2004, route des Lucioles - BP 93 - 06902 Sophia Antipolis Cedex (France)

Unité de recherche INRIA Futurs : Parc Club Orsay Université - ZAC des Vignes
4, rue Jacques Monod - 91893 ORSAY Cedex (France)
Unité de recherche INRIA Lorraine : LORIA, Technopôle de Nancy-Brabois - Campus scientifique
615, rue du Jardin Botanique - BP 101 - 54602 Villers-lès-Nancy Cedex (France)
Unité de recherche INRIA Rennes : IRISA, Campus universitaire de Beaulieu - 35042 Rennes Cedex (France)
Unité de recherche INRIA Rhône-Alpes : 655, avenue de l'Europe - 38334 Montbonnot Saint-Ismier (France)
Unité de recherche INRIA Rocquencourt : Domaine de Voluceau - Rocquencourt - BP 105 - 78153 Le Chesnay Cedex (France)

Éditeur
INRIA - Domaine de Voluceau - Rocquencourt, BP 105 - 78153 Le Chesnay Cedex (France)
http://www.inria.fr
ISSN 0249-6399